https://doi.org/10.1016/j.buildenv.2012.02.027 This is the Pre-Published Version.

An Experimental Study of Bioaerosol (1-10 μm) Deposition in a Ventilated Chamber

A.C.K. Lai[a], L.T. Wong[b], K.W. Mui[b*], W.Y. Chan[b], H.C. Yu[b]

[a]Department of Civil and Architectural Engineering, City University of Hong Kong,

Tat Chee Avenue, Kowloon, Hong Kong, China

[b]Department of Building Services Engineering, The Hong Kong Polytechnic University,

Hong Kong, China

[*]Corresponding author: K.W. Mui

E-mail: behorace@polyu.edu.hk; Tel: (852) 2766 5835; Fax: (852) 2765 7198

ABSTRACT

Understanding of bioaerosols deposition in ventilated environments can significantly improve our current knowledge on exposure. This study presents an experimental and numerical analysis for bioaerosol deposition in a scaled ventilation chamber. Three different group sizes of common indoor airborne bioaersols ranging from 1 to 10 μm, (*Micrococcus luteus*, *Staphylococcus aureus*), (*Aspergillus niger*, *Penicillium citrinum*) and (*Rhizopus* sp.), were atomized and injected to a small chamber with three controllable ventilation flow rates varying from 1.7 h^{-1} to 18.8 h^{-1}. Twenty-eight (7 × 4) Petri dishes were placed at the bottom of the chamber and deposition was counted after inoculation. A commercial computational fluid dynamics tool was used to predict bioaerosol deposition. The results were compared with experiments and satisfactory agreements between them were observed. The results reveal that the larger the aerosol size, the shorter the deposition distance away from the inlet. The comparisons are further improved if non-spherical shape factor is considered.

Keywords: experimental and numerical analysis; 1 to 10 μm bioaerosol deposition; scaled ventilation chamber; controllable ventilation flow rates.

Nomenclature:

CFD	computational fluid dynamics
CFU	colony forming unit
RNG	renormalization group
T	absolute temperature of the fluid
Re	Reynolds number
Re_{sph}	Reynolds number computed with the diameter of a sphere
b_1, b_2, b_3, b_4	coefficient as defined in Equation (3)
C_c	Cunningham slip correction factor
C_D	drag coefficient
C_{ij}	fractional count of bioaerosols
C_i	longitudinal fractional counts
C_j	fractional counts along the meridian direction
d_p	particle diameter
d_{lk}, d_{kl}, d_{ij}	deformation rate tensors
$F_D(u-u_p)$	drag force per unit particle mass
F_{Brownian}	Brownian Force
F_x	additional acceleration
	Saffman's lift force
g	gravity force
h^{-1}	per hour
ij	array coordinates
	constant, 2.594
k_B	Boltzmann constant
MEA	Malt Extract Agar
u_p	particle velocity
u	fluid parcel velocity
TSA	Tryptone Soya Agar
TSB	Tryptone Soya Broth
V_R	ventilation rate
ρ_p	particle density
ρ	carrier phase density
μ	molecular viscosity of the carrier phase
ϕ	particle sphericity
S_o	spectral intensity
ν	kinematic viscosity

	zero-mean, unit-variance independent Gaussian random number
Δt	time step
$\sqrt{\overline{u_i^2}}$	root mean square (RMS) local fluctuation velocity in the *i*-th direction
Φ_{ij}	total counts of bioaerosols at location *ij*
ω	deposition ratio in the chamber

1. INTRODUCTION

Airborne transmission of pathogenic bioaerosols poses threat to public health. An understanding of the distribution and deposition of bioaerosols is an important mean for controlling airborne infections in indoor environments. Since the outbreak of airborne viruses such as SARS and influenza A (H1N1) in the recent years, relevant studies, that include the estimation of indoor airborne virus exposure and the modeling of exhaled droplet nuclei dispersion indoors, have been mounting [1-3].

Deposition is an important and efficient process to remove indoor contaminants [4]. It has been shown that fungal materials, heavy metals, viable biological particles are found in settled dust [5,6]. Recent study reported the correlation between the resuspension of indoor aeroallergens to lung inflammation in asthmatic children [7]. Measurements have also shown that different particle sizes can be detached and resuspended from the floors effectively [5,8]. Hence it is very important to quantify the deposition rate for indoor environments, particularly for floor surface which is susceptible to particle resuspension. A review on particle deposition indoors [9] has highlighted and addressed that many particle loss experiments measured total loss and no differentiation on wall orientation was made [10-16].

In literature there are studies on experimental and numerical investigations of indoor particle deposition. Most of these deposition studies measured particle loss rate [14-16]. Direct deposition measurement is scarce [8,9,17].In order to have a more accurate exposure assessment, it is very important to know where the particles lost inside the indoor environment. Direct deposition measurement can provide such information but it is very tedious as sufficient particles must be collected before counting [17-18]. Various techniques such as neutron activation

analysis [19] and fluorescent analysis [20] to measure deposition onto smooth and rough surfaces have been reported. With the advances of computer technology, computational fluid dynamics (CFD) has become another powerful tool for studying particle deposition [21-24]. It is convenient to accurately control particle parameters (size, density, shape, etc.), making numerical investigations feasible, when considering all factors influencing the deposition rate.

All the previous experiments and modeling studies on particle deposition considered spherical particles only and did not distinguish between non-biological particles and biological aerosols in terms of airborne transmission mechanism. Indeed, not much conclusive information focused on the aerodynamic properties of indoor bioaerosol transmission is available.

In addition to the wide range of bacterial and fungal bioaerosols on record (with aerodynamic diameters ranging from 0.3 to 11 μm) [25,26], non-spherical particles in indoor air might have significant drag influences on the particle concentration, settling velocity and deposition pattern in a forced ventilated environment [9,27-29]. This paper highlighted the influence of aerosol size on the deposition distance and compared with the previous study in which only one type of bacteria was generated and the focus was put on how influence of the ventilation rate on deposition distance [30]. In this study, various sizes of bioaerosols were tested and the shape factor was also considered. Deposition on the floor was examined both experimentally and numerically using CFD.

2. METHODOLOGY

2.1 Experiments

The groups of common indoor airborne (culturable) bioaerosols chosen in this study were in three cell diameters d_p: (1) bacteria with d_p=0.8-1.2 μm (*Micrococcus luteus*, American Type Culture Collection ATCC 4698 and *Staphylococcus aureus*, ATCC 6538); (2) fungi with d_p=3-4 μm (*Aspergillus niger*, *Penicillium citrinum*, ATCC 6849); and (3) fungi with d_p=10 μm (*Rhizopus* sp.). All of the bioaerosols were globose, ovoid or elliptical, and their compound light microscope images are shown in Figure 1. *Micrococcus* and *Staphylococcus* (Group 1), gram-positive cocci, are common indoor contaminants shed from human skin surface. In terms of airborne bacterial composition, they equaled 38% in a survey of 100 US buildings while 100% in a Poland housing study [31,32]. *Aspergillus, Penicillium* (Group 2) and *Rhizopus* (Group 3) are fungal genera found indoors which can be transported from outdoors and generated from contaminated building materials [33]. Some species of these genera are associated with allergy, hypersensitivity pneumonitis, toxic or irritant reaction, and direct infection (e.g. *Aspergillosis*, *Zygomycosis*) [34].

<< Figure 1. Three groups of reference bioaerosols>>

A method for the preparation of vegetative bacterial cells for Group 1 and fungal spore suspensions for Groups 2 and 3 was as follows [35-37]. Initially, the bacterial cultures were inoculated onto Tryptone Soya Agar (TSA; Oxoid, Hampshire, UK) and incubated at 30°C for 24 hours. A single colony was then picked from the TSA, inoculated into 10 ml Tryptone Soya Broth (TSB; Oxoid, Hampshire, UK) and incubated at 30°C under aerobic conditions for another

24 hours. Similarly, the fungal cultures were inoculated onto 2% Malt Extract Agar (MEA; Oxoid, Hampshire, UK) and incubated at 25°C for 1 week. After that, a single colony was picked and inoculated onto another 2% MEA plate which in turn was incubated at 25°C for a further week. For Groups 1 and 2, a 50 ml bacterial/fungal suspension was stored in a collision nebulizer (BGI Inc., Waltham, MA) for aerosolization. By spreading its serially diluted samples (made in sterilized Ringer's solution) onto agar plates for counting after incubation, the suspension was tested for sufficient amount of viable cells. In this study, the average concentrations of the bacterial and fungal suspensions were 6×10^5 CFU ml^{-1} and 2×10^4 CFU ml^{-1}, respectively. For Group 3, a small chamber of size 0.145 m (L) × 0.145 m (W) × 0.065 m (H) with a mixing fan, through which an air jet was directed to the cultured fungi (from diluted suspension of 240 spores on 20-mm thick MEA) placed on the chamber floor, was used for aerosolization.

Figure 2 shows the experimental setup for testing the bioaerosol deposition distribution patterns. A 70L tempered glass ventilated chamber of size 0.650 m (L) × 0.380 m (W) × 0.284 m (H) was sealed and placed inside a Class II biological safety cabinet. The leakage rate tested under air pressure was 2.4×10^{-3} min^{-1}. A total of 28 agar plates (i.e. TSA for bacteria and MEA for fungi) organized in an array of 7 columns by 4 rows were laid on the chamber floor to record the deposition patterns.

<< Figure 2. Experimental setup >>

During the study, compressed air, first filtered through an air filtration system "a" (Model 3074B, TSI) for moisture and impurities removal, entered the cabinet via two airflow paths f_1 (variable flow rates) and f_2 (a constant flow rate of 2 L min^{-1}) and then passed into airflow path f_3. f_1 was for the adjustment of aerosol concentration by volume while f_2, connected to a 6-jet

collision nebulizer "c" for Groups 1 and 2 or to an aerosolization chamber for Group 3, was for the generation of bioaerosols. The volume flow rates in f_1, f_2 and f_3 could be conditioned and were gauged by flow meters "b_1", "b_2" and "b_3", respectively. Moisture was removed again in f_3 via a diffusion dryer "d" (Model 3062, TSI). The processed air was finally supplied to the chamber through a high sidewall inlet "e_1" and exhausted through an outlet "e_2" aligned on the opposite chamber wall. Both the inlet and outlet were circular with a diameter of 0.016 m. Measurements were conducted at ventilation rates of 1.7 h^{-1}, 10.3 h^{-1} and 18.8 h^{-1}, corresponding to inlet velocities of 0.17 ms^{-1}, 1.0 ms^{-1} and 1.8 ms^{-1},respectively. It was noted that 1-20 h^{-1} was a typical ventilation rate range for enclosures and the selected composition was one of the common ventilation configurations [38]. Test procedures were adopted for the chamber to achieve isothermal conditions at an air temperature of 25°C and a relative humidity of 55%.

Experiments of deposition distribution were started within one hour after the preparation of bioaerosols for viability. For each deposition distribution test, bioaerosols were supplied into the chamber through inlet "e_1" for 60 minutes in the form of an isothermal air jet. Air samples (each of 0.1 m^3) in the chamber were collected by Biostage Single-stage Viable Cascade Impactors before and after the experiments to ensure steady state condition. Sample tests did show insignificant concentration trend during the sampling periods ($p \geq 0.3$, t-test). The chamber plates were collected and colonies on each plate were inspected every day during the incubation period for colony counting. The bioaerosol particles, which were transferred onto microscope slides using transparent adhesive tape, were scrutinized to verify the assumption that each colony formed on agar plates arises from one cell. There was no airborne mycelium found in the experiments.

The chamber was sterilized before and after each measurement by 75% ethanol and a 30-min ultraviolet light irradiation. Air samples collected for airborne bacterial and fungal counts were used to examine the chamber cleanliness.

2.2 Numerical model

The bioaerosol deposition patterns in the chamber were simulated using a commercial finite volume based CFD code FLUENT (version 6.3) based on an Eulerian-Lagrangian approach. Convection term was discretized by the second-order upwind scheme. The PISO algorithm was adopted to couple the pressure and velocity fields. Renormalization group (RNG) k-ε model, whose details are presented in a previous study [30], was selected to model turbulent flow. A grid system with mesh size 320 k (grid convergence index 4.9%) was used [39]. As the deposition process was very slow, the airflow and particle motion were modeled under steady-state conditions.

The transport of the discrete phase was modeled by a Lagrangian scheme. In the simulations, tracer particles of diameters 1, 4 and 10 μm were injected continuously through the inlet for Groups 1, 2 and 3, respectively. Bioaerosol concentrations in the chamber were kept at a low volume fraction (<5,500 CFU m^{-3}). With this low concentration, the effect of particles on turbulent flow and the coagulation of bioaerosols could be neglected. Each particle released from the injection site was tracked separately for its position, velocity and residence time. The motion of a particle can be calculated by integrating the force balance on the particle in terms of drag,

gravity, g and additional acceleration, F_x as given by Equation (1) below, where u_p and u are the particle and fluid parcel velocities, ρ_p and ρ are the particle and carrier phase densities, respectively. It was noted that a range of bioaerosol densities from 1.1 to 1.3 g cm^{-3} was found to have insignificant influence on the deposition patterns in the chamber [30]. Hence, in this study, it was assumed to be (=1.1 g cm^{-3}).

$$\frac{du_p}{dt} = F_D(u - u_p) + \frac{g(\rho_p - \rho)}{\rho_p} + F_x \quad \ldots (1)$$

$F_D(u_p - u)$ is the drag force per unit particle mass and F_D is defined as, where μ is the molecular viscosity of the carrier phase, d_p is the particle diameter, and Re is the Reynolds number,

$$F_D = \frac{18\mu}{d_p^2 \rho_p} \frac{C_D Re}{24}; \; Re = \frac{\rho d_p |u_p - u|}{\mu} \quad \ldots (2)$$

In this study, influences of the surface roughness of bioaerosols are approximated by Reynolds number computed with the diameter of a sphere, $\mathrm{Re_{sph}}$ and the particle sphericity ϕ, the corresponding drag coefficient C_D can be determined as follows [29,40],

$$C_D = \frac{24}{\mathrm{Re_{sph}}}(1 + b_1 \mathrm{Re_{sph}}^{b_2}) + \frac{b_3 \mathrm{Re_{sph}}}{b_4 + \mathrm{Re_{sph}}}; \; b_1 = \exp(2.3288 - 6.4581\phi + 2.4486\phi^2); \; b_2 = 0.0964 + 0.5565\phi; \; b_3 = \exp(4.905 - 13.8944\phi + 18.4222\phi^2 - 10.2599\phi^3); \; b_4 = \exp(1.4681 + 12.2584\phi - 20.7322\phi^2 + 15.8855\phi^3) \quad \ldots (3)$$

At low airflow rates, the Brownian force that affects the particle motion is given by the following equation [41], where S_o is the spectral intensity, is a zero-mean, unit-variance independent Gaussian random number, k_B is the Boltzmann constant, T is the absolute temperature of the fluid, C_c is the Cunningham slip correction factor, and Δt is the time step,

$$F_{\text{Brownian}} = \varsigma_i \sqrt{\frac{\pi S_o}{\Delta t}}\ ;\ S_o = \frac{216\nu k_B T}{\rho d_p^5 (\rho_p / \rho)^2 C_c} \qquad \ldots (4)$$

For the consideration of Saffman's lift force , or lift due to shear, can be included in the additional force term as shown in Equation (5) [41], where = *2.594*, and d_{lk}, d_{kl}, d_{ij} are the deformation rate tensors.

$$F_{Lift} = \frac{2K_L \nu^{1/2} \rho d_{ij}}{\rho_p d_p (d_{lk} d_{kl})^{1/4}} (u - u_p) \qquad \ldots(5)$$

Instantaneous particle velocity is determined by the application of a discrete random walk model and by assuming that the fluctuation velocities follow a Gaussian probability distribution as shown below, where $\sqrt{\overline{u_i^2}}$ is the root mean square (RMS) local fluctuation velocity in the *i*-th direction,

$$u_i' = \varsigma_i \sqrt{\overline{u_i^2}} \qquad \ldots(6)$$

This model assumes successive encounter of particles with discrete turbulence eddies and the eddy interaction time scale can be found elsewhere [42]. In the study, deposition was assumed for all particles touching a surface and no resuspension was considered.

2.3 Deposition patterns

Non-homogeneous deposition distribution patterns of the bioaerosols in both experimental and numerical studies are expressed by the fractional count C_{ij} presented in Equation (7) below, where Φ_{ij} is the total counts at location ij, i=1…7 and j=1…4 are the array coordinates corresponding to the chamber fractional length x/L=0.069, 0.208, 0.346, 0.485, 0.623, 0.762, 0.9 and the chamber fractional width y/W=0.125, 0.375, 0.625, 0.875, respectively.

$$C_{ij} = \frac{\Phi_{ij}}{\sum_i \sum_j \Phi_{ij}} \quad \ldots (7)$$

Uniformity of the longitudinal deposition patterns can be evaluated by Chi-square test [43]. The longitudinal deposition patterns are the longitudinal fractional counts C_i along x/L at *i* in relation to the expected counts at *j*,

$$C_i = \frac{\sum_j \Phi_{ij}}{\sum_i \sum_j \Phi_{ij}} \quad \ldots (8)$$

The deposition ratio in the chamber ω is a measure to present the longitudinal spatial distribution pattern and can be expressed by,

$$\omega = \frac{\sum_{i=5}^{7} C_i}{\sum_{i=1}^{3} C_i} \quad \ldots (9)$$

3. RESULTS AND DISCUSSION

The deposition distributions under 15 test conditions, i.e. the five bioaerosol species (*S. aureus*, *M. luteus*, *A. niger*, *P. citrinum* and *Rhizopus* sp.) divided into Groups 1-3 and sampled at the three ventilation rates (V_R=1.7 h^{-1}, 10.3 h^{-1} and 18.8 h^{-1}), were measured from two to four repeated experiments. As the deposition patterns would be dominated by not only the airflow conditions but also the gravitational and drag forces acted on the bioaerosols, the size was selected to be an explanatory parameter in this study.

Figure 3 presents the average fractional counts C_{ij} measured on the agar plate array. Larger fractional count variations were observed along the longitudinal direction (i.e. i along x-axis), as compared with the meridian direction (i.e. j along y-axis). Significant trends were reported for longitudinal fractional counts (C_i) in all ($p \leq 0.05$, t-test), except 2-out-of-3 experimental cases with *Micrococcus* ($p=0.2$, t-test) whereas insignificant trends were reported for the fractional counts along the meridian direction (C_j) in over 95% of the measurement cases ($p>0.05$, t-test). Besides, the C_j values in more than 80% of the measurement cases were normally distributed ($p \geq 0.05$, Shapiro-Wilk test). Longitudinal spatial deposition patterns were therefore simulated and the results are summarized in Figure 4 and Table 1. CFD particle tracking results for spherical particles with sphericity $\phi = 1$ are shown for comparison.

<< Figure 3. Average fractional counts (C_{ij}) measured on the agar plate array>>

<< Figure 4. Longitudinal fractional counts C_i on the test chamber floor measured at three ventilation rates>>

<<Table 1 Experimental and computational fractional count results>>

The longitudinal deposition patterns were found to be non-uniform for Group 1 at all ventilation rates V_R and Group 2 except one case (*Aspergillus niger*) at ventilation rate V_R=10.3 h^{-1} ($p \leq 0.02$, Chi-square test). They were found non-uniform for Group 3 as well ($p \leq 0.0001$, Chi-square test). Simulations confirmed the experimental results qualitatively: non-uniform longitudinal deposition patterns were revealed ($p<0.03$, Chi-square test) for the particle size range between 1 μm and 10 μm, except for the 4 μm particles at the smallest ventilation rate of 1.7 h^{-1}, and for the 10 μm particles at ventilation rate V_R=10.3 h^{-1}. This outcome qualitatively agreed with the general understanding of particle deposition [9,27,28,44,45]. At the same time, it confirmed that the spatial distribution of bioaerosols in a ventilated space was related to the particle size and ventilation rate [30].

Theoretically, the settling velocity is proportional to the square of particle size, and the movement of small sized particles is strongly influenced by airflow while the movement of large sized particles is dominated by gravity. The higher the inlet velocity (indicated by the ventilation rate), the higher is the air jet momentum and thus a larger deposition distance from the inlet [38,44]. In this study, smaller sized bioaerosols (Group 1) tended to deposit near the outlet (i.e. larger deposition distance) while the larger ones (Group 3) tended to deposit close to the inlet (i.e. smaller deposition distance). Increased deposition near the outlet under the conditions of higher jet momentum in groups 1&2 was due to increased particle collisions with the chamber walls [36]. In this study, particle sizes between 1 μm and 10 μm under the ventilation rate ranges from 1.7 h^{-1} to 18.8 h^{-1} were selected. Using the density of 1.1 g cm^{-3} [30], the settling velocity ranges from 3.85×10^{-5} ms^{-1} to 3.41×10^{-3} ms^{-1} and the loss rate due to gravitational settling is ranged from 0.97 h^{-1} to 85.8 h^{-1} for 1 μm and 10 μm respectively. The significant lost rate is attributed to the chamber height. However it should be noted that in practical indoor environments, the

room height is approximately 2 m and the loss rate will be changed to 0.14 h^{-1} to 12.27 h^{-1} respectively. Hence in practice, deposition lost rate of coarse bioaerosols is comparable to the ventilation rate and is an important factor affecting exposure.

Both of the experimental and computational results showed significant trends ($p \leq 0.05$, t-test) of longitudinal fractional counts (i.e. C_i against x/L) overall. The exceptions were two experimental cases of *M. luteus* in Group 1 (p=0.17-0.20, t-test) and 2 computational cases of Group 2 at the lowest ventilation rate (p=0.26-0.99, t-test) and Group 3 spherical particles (ϕ =1) at the ventilation rate V_R=10.3 h^{-1} (p=0.16-0.81, t-test). Slopes of the longitudinal fractional counts against the fractional length x/L were reported positive and to be increasing with the ventilation rate V_R for Groups 1 and 2, yet for Group 3 from negative to positive.

The exclusion of Saffman's lift force in simulations presented no difference on the longitudinal fractional counts ($p \geq 0.9$, Chi-square test), except for 5 cases at the ventilation rate V_R=10.3 h^{-1} (p=0.65-0.87, Chi-square test) presented no significant differences. In the present case, despite of the bioaerosol tested was up to 10 μm, the low velocity resulted in low relaxation time. From the literature it is clearly shown that Saffman lift force play role in inertia-moderated regime only [46-48]. No difference on the longitudinal fractional counts between particles of sphericity ϕ =0.2-1 in simulations for Groups 1 and 2 cases were reported ($p \geq 0.9$, Chi-square test). Simulation results for Group 3 showed significant difference in lowest ventilation rate ($p \leq 0.0001$, Chi-square test) and some differences for higher ventilation rates (p=0.05-0.25, Chi-square test).

Figure 5 illustrates the deposition ratios ω (Table 1) against the ventilation rate V_R (with error bars of one standard deviation). The fractional counts C_i at i=4 were not included in the

ratio calculation as they were not significantly different from the expected counts ($p>0.1$, t-test). Slopes were positive for all Groups from both of the experiments and computations except a negative slope for Group 3 experiment. As smaller particles were expectedly predominated by airflow, there were significant correlations ($p\leq0.03$, t-test) for Group 1 (smaller size) yet insignificant correlations ($p\geq0.2$, t-test) for Group 3 (larger size). The ventilation rates tested had very little effect on the deposition ratios of Group 3. Although correlation was found computationally ($p=0.03$, t-test) for Group 2, insufficient experimental data was available for verification ($p=0.4$, t-test).

<< Figure 5. Deposition ratios for the three groups>>

With respect to the general trend of deposition ratio, once again, the numerical model for spherical solid particles predicted the experimental deposition patterns qualitatively. In some cases, however, the predicted deposition ratios could be 2 times higher for Groups 1 and 2 or 40% lower for Group 3.

Inferring from the SEM photos, it can be seem that the morphology of the tested bioaerosols are far from ideal smooth and spherical presumption. It will affect the drag forces experienced by the particles. In FLUENT, this can be incorporated into "shape factor". Since the drag of non-solid and non-smooth bioaerosol particles would be approximated by the particle sphericity in the numerical model, simulation results for an extreme sphericity $\phi=0.2$ were shown in Figure 5 for illustration. The drag coefficient for a non-spherical particle depends on particle Reynolds number. For the particle size tested in this work, the expected Reynolds number would be in the order of 1. According to the previous results [40], the ratio of the drag coefficient of non-spherical to spherical particle would be in the range of 1 to 5 within the Reynolds number

range of this study. Expectedly, the computational results as shown in Figure 4 demonstrated that in all simulation cases, the larger the bioaerosols, further of the deposition distance measured from the inlet. Figure 5 also depicts the corresponding deposition ratios of the extreme cases where ϕ=0.2. It was noted that the inclusion of drag force would improve the predictions for bioaerosols at low ventilation rates. Information on drag coefficients for bioaerosol particles, on the other hand, would need further research.

The discrepancy between the modeling and experimental results could be partly attributed to the simplified deposition surface in the model. In the current CFD, the chamber bottom was assumed to be smooth while in the actual experiments, 28 Petri dishes were put on the bottom to collect the samples. Each dish is about 8.8 cm in diameter and the edge is about 1.2 cm height. The array of 7 × 4 dishes disturb the airflow near wall which might affect deposition rate.

4. CONCLUSION

Particle aerodynamics in forced ventilated environments is an important factor for understanding airborne disease dispersion and deposition. In this study, multiple depositions of bioaerosols with three different sizes ranged between 0.8 μm and 10 μm in a forced ventilated chamber were investigated with ventilation rates varying from 1.7 h^{-1} to 18.8 h^{-1}. Using an earlier presented CFD model, the deposition distributions inside the chamber could be qualitatively predicted. The results confirmed that movement of small sized bioaerosols is strongly influenced by airflow while movement of large sized bioaerosols is dominated by gravity. Hence, the inclusion of drag force would improve the prediction of deposition distance in the chamber particularly for bioaerosol particles at low ventilation rates.

ACKNOWLEDGMENT

The work described in this paper was partially supported by grants from The Hong Kong Polytechnic University (Project account numbers G-U909, G-SA04 and YK22) and The City University of Hong Kong (Project number 7002273).

REFERENCES

[1] Chao CYH, Wan MP, Sze To GN. Transport and removal of expiratory droplets in hospital ward environment. Aerosol Sci Technol 2008;42(5):377–94.

[2] Sze To GN, Wan MP, Chao CYH, Wei F, Yu SCT, Kwan JKC. A methodology for estimating airborne virus exposures in indoor environments using the spatial distribution of expiratory aerosols and virus viability characteristics. Indoor Air 2008;18(5):425–38.

[3] Mui KW, Wong LT, Wu CL, Lai ACK. Numerical modeling of exhaled droplet nuclei dispersion and mixing in indoor environments. J Hazard Mater 2009;167(1–3):736–44.

[4] Lai ACK, Nazaroff WW. Modeling indoor particle deposition from turbulent flow onto smooth surfaces. J Aerosol Sci 2000;31(4):463–76.

[5] Qian J, Ferro AR. Resuspension of dust particles in a chamber and associated environmental factors. Aerosol Sci Technol 2008;42(7):566–78.

[6] Lioy PJ, Freeman NCG, Millette JR. Dust: A metric for use in residential and building exposure assessment and source characterization. Environ Health Perspect 2002; 110(10):969–83.

[7] Raja S, Xu Y, Ferro AR, Jaques PA, Hopke PK. Resuspension of indoor aeroallergens and relationship to lung inflammation in asthmatic children. Environ Int 2010;36(1):8–14.

[8] Thatcher TL, Fairchild WA, Nazaroff WW. Particle deposition from natural convection enclosure flow onto smooth surfaces. Aerosol Sci Technol 1996;25(4):359–74.

[9] Lai ACK. Particle deposition indoors: a review. Indoor Air 2002;12(4):211–14.

[10] Morawska L, Jamriska M. Deposition of radon progeny on indoor surfaces. J Aerosol Sci 1996;27(2):305–12.

[11] Nomura Y, Hopke PK, Fitzgerald B, Mesbah B. Deposition of particles in a chamber as a function of ventilation rate. Aerosol Sci Technol 1997;27(2):62–72.

[12] Van Dingenen R, Raes F, Vanmarcke H. Molecule and aerosol particle wall losses in SMOG chambers made of glass. J Aerosol Sci 1989;20(1):113–22.

[13] Xu M, Nematollahi M, Sextro RG, Gadgil AJ, Nazaroff WW. Deposition of tobacco smoke particles in a low ventilation room. Aerosol Sci Technol 1994;20(2):194–206.

[14] Abadie M, Limam K, Allard F. Indoor particle pollution: effect of wall textures on particle deposition. Build Environ 2001;36(7):821–7.

[15] Hussein T, Hruska A, Dohanyosova P, Dzumbova L, Hemerka J, Kulmala M, et al. Deposition rates on smooth surfaces and coagulation of aerosol particles inside a test chamber. Atmos Environ 2009;43(4):905–14.

[16] He CR, Morawska L, Gilbert D. Particle deposition rates in residential houses. Atmos Environ 2005;39(21):3891–9.

[17] Lai ACK, Nazaroff WW. Supermicron particle deposition from turbulent chamber flow onto smooth and rough vertical surfaces. Atmos Environ 2005;39(27):4839–900.

[18] Lai ACK, Byrne MA, Goddard AJH. Experimental studies of the effect of rough surfaces and air speed on aerosol deposition in a test chamber. Aerosol Sci Technol 2002;36(10):973–82.

[19] Lai ACK, Byrne MA, Goddard AJH. Measured deposition of aerosol particles on a two-dimensional ribbed surface in a turbulent duct flow. J Aerosol Sci 1999;30(9):1201–14.

[20] Thatcher TL, Lai ACK, Moreno-Jackson R, Sextro RG, Nazaroff WW. Effects of room furnishings and air speed on particle deposition rates indoors. Atmos Environ 2002;36(11): 1811–9.

[21] Tian L, Ahmadi G. Particle deposition in turbulent duct flows–comparisons of different model predictions. J Aerosol Sci 2007;38(4):377–97.

[22] Zhang Z, Chen Q. Experimental measurements and numerical simulations of particle transport and distribution in ventilated rooms. Atmos Environ 2006;40(18):3396–408.

[23] Zhao B, Chen C, Tan Z. Modeling of ultrafine particle dispersion in indoor environments with an improved drift flux model. J Aerosol Sci 2009;40(1):29–43.

[24] Wang M, Lin C-H, Chen Q. Determination of particle deposition in enclosed spaces by Detached Eddy Simulation with the Lagrangian method. Atmos Environ 2011;45(30):5376–84.

[25] Cox CS, Wathes CM. Bioaerosols in the Environment. In: Bioaerosols handbook. Boca Raton: CRC Press Inc.; 1995.

[26] Samson RA, Hoekstra ES, Frisvad JC, Filtenborg O. Introduction to food– and airborne fungi. 6th ed. Utrecht: Centraalbureau voor Schimmelcultures; 2002.

[27] Nazaroff WW. Indoor particle dynamic. Indoor Air 2004;14(7):175–83.

[28] Bouilly J, Limam K, Béghein C, Allard F. Effect of ventilation strategies on particle decay rates indoors: An experimental and modeling study. Atmos Environ 2005;39 (27):4885–92.

[29] Loth E. Drag of non-spherical solid particles of regular and irregular shape. Powder Technol 2008;182(3):342–53.

[30] Wong LT, Chan WY, Mui KW, Lai ACK. An experimental and numerical study on deposition of bioaerosols in a scaled chamber. Aerosol Sci Technol 2010;44(2):117–28.

[31] Górny RL, Dutkiewicz J. Bacterial and fungal aerosols in indoor environment in Central and Eastern European countries. Ann Agr Env Med 2002;9(1):17–23.

[32] Tsai FC, Macher JM. Concentrations of airborne culturable bacteria in 100 large US buildings from the BASE study. Indoor Air 2005;15(S9):71–81.

[33] Gots RE, Layton NJ, Pirages SW. Indoor Health: Background levels of fungi. AIHA J 2003;64(4):427–38.

[34] Castón-Osorio JJ, Rivero A, Torre-Cisneros J. Epidemiology of invasive fungal infection. Int J Antimicrob Agents 2008;32(2):S103–9.

[35] Agranovski V, Ristovski Z, Hargreaves M, Blackall PJ, Morawska L. Real-time measurement of bacterial aerosols with the UVAPS: performance evaluation. J Aerosol Sci 2003;34(3):301–17.

[36] Kanaani H, Hargreaves M, Smith J, Ristovski Z, Agranovski V, Morawska L. Performance of UVAPS with respect to detection of airborne fungi. J Aerosol Sci 2008;39(2):175–89.

[37] Kanaani H, Hargreaves M, Ristovski Z, Morawska L. Deposition rates of fungal spores in indoor environments, factors effecting them and comparison with non-biological aerosols. Atmos Environ 2008;42(30):7141–54.

[38] Chow WK, Wong LT. Air diffusion terminal devices: macroscopic numbers describing jet momentum. Build Serv Eng Res Technol 1998;19(1):49–54.

[39] Roache PJ. Verification of codes and calculation. AIAA J 1998;36(5):696–702.

[40] Haider A, Levenspiel O. Drag coefficient and terminal velocity of spherical and non-spherical particles. Powder Technol 1989;58(1):63–70.

[41] Li A, Ahmadi G. Dispersion and deposition of spherical particles from point sources in a turbulent channel flow. Aerosol Sci Technol 1992;16(4):209–26.

[42] FLUENT. FLUENT 6.3 User's Guide. Lebanon: Fluent Inc.; 2006.

[43] Kanji GK. 100 statistical tests. 3rd ed. London: Sage publications; 2006. [44] Hinds WC. Aerosol technology: properties, behavior, and measurement of airborne particles. 2nd ed. New York: John & Wiley & Sons Inc.; 1999.

[45] Zhao B, Wu J. Effect of particle spatial distribution on particle deposition in ventilation rooms. J Hazard Mater 2009;170(1):449–56.

[46] Young J, Leeming A. A theory of particle deposition in turbulent pipe flow. J Fluid Mech 1997;340:129-59.

[47] Guha, A. A unified Eulerian theory of turbulent deposition to smooth and rough surfaces. J Aerosol Sci 1997;28(8):1517–37.

[48] Chen Q, Ahmadi G. Deposition of particles in a turbulent pipe flow. J Aerosol Sci 1997;28(5):789-96.

Table 1 Experimental fractional count results

Case	Ventilation rate V_R (h^{-1})	Trials N	Fractional count (C_i) of fractional distance from air inlet (x/L)							Deposition ratio ω
			***i*=1**	**2**	**3**	**4**	**5**	**6**	**7**	
			0.07	**0.21**	**0.35**	**0.49**	**0.62**	**0.76**	**0.90**	
Group 1 (d_p=0.8 μm to 1.2 μm)										
S. aureus	1.7	2	0.131	0.115	0.115	0.132	0.138	0.167	0.201	1.40
	10.3	3	0.105	0.113	0.127	0.145	0.154	0.168	0.188	1.48
	18.8	3	0.104	0.097	0.1	0.129	0.183	0.182	0.204	1.89
M. luteus	1.7	3	0.139	0.133	0.128	0.159	0.139	0.143	0.160	1.10
	10.3	2	0.099	0.107	0.143	0.161	0.164	0.167	0.159	1.41
	18.8	2	0.096	0.105	0.141	0.190	0.172	0.168	0.129	1.37
Group 2 (d_p=3 μm to 4 μm)										
P. citrinum	1.7	3	0.126	0.125	0.136	0.14	0.147	0.162	0.165	1.22
	10.3	3	0.121	0.119	0.124	0.147	0.148	0.16	0.181	1.34
	18.8	3	0.080	0.093	0.123	0.146	0.175	0.192	0.192	1.89
A. niger	1.7	4	0.115	0.11	0.133	0.141	0.159	0.164	0.177	1.39
	10.3	4	0.130	0.135	0.140	0.137	0.148	0.157	0.154	1.13
	18.8	3	0.082	0.103	0.135	0.154	0.203	0.177	0.145	1.64
Group 3 (d_p=10 μm)										
Rhizopus sp.	1.7	4	0.185	0.163	0.138	0.152	0.133	0.117	0.113	0.75
	10.3	3	0.181	0.184	0.162	0.145	0.113	0.111	0.105	0.62
	18.8	3	0.165	0.177	0.155	0.152	0.124	0.113	0.113	0.70

Figure

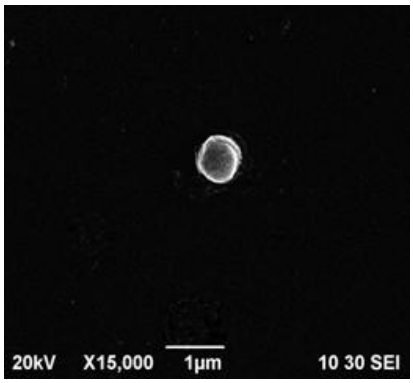

S. aureus

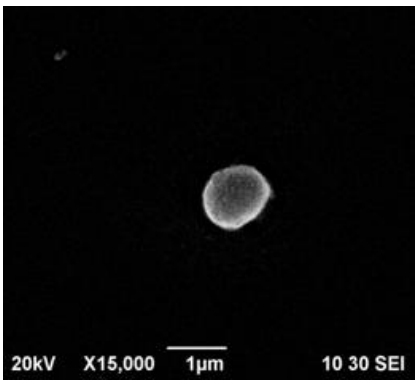

M. luteus

Group 1 (d_p=0.8μm to 1.2μm)

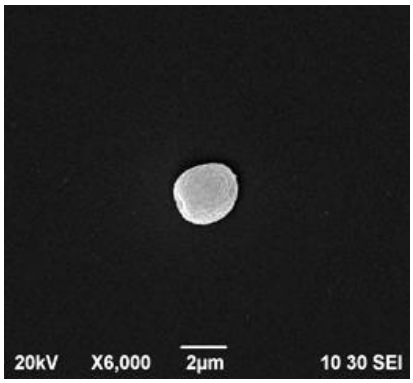

P. citrinum

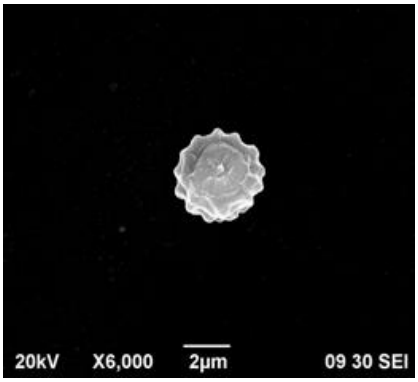

A. niger

Group 2 (d_p=3 μm to 4 μm)

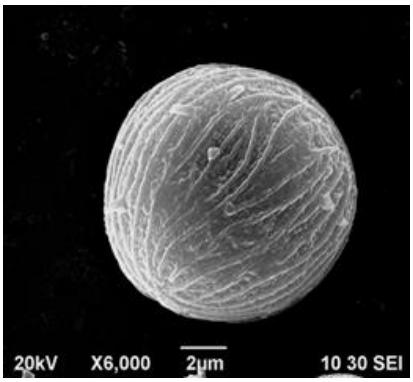

Rhizopus sp.

Group 3 (d_p=10 μm)

Figure 1. Three groups of reference bioaerosols

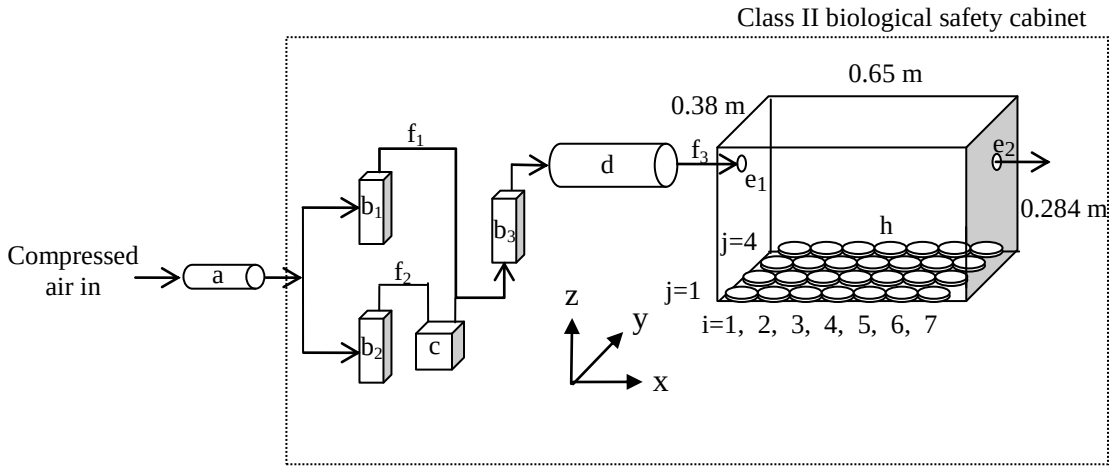

a	filtration system	d	diffusion dryer
b	flow meter	e_1	inlet
c	6-jet collision nebulizer or aerosolization chamber for *Rhizopus* sp.*	e_2	outlet
		f	airflow path
		h	agar plate array in i=1…7 columns by j=1…4 rows

* Details of aerosolization chamber "c" for *Rhizopus* sp.

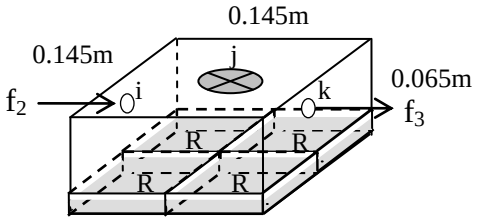

i	inlet of chamber (diameter - 0.009m)
j	mixing fan
k	outlet of chamber (diameter - 0.009m)
R	*Rhizopus* sp. on agar

Figure 2. Experimental setup

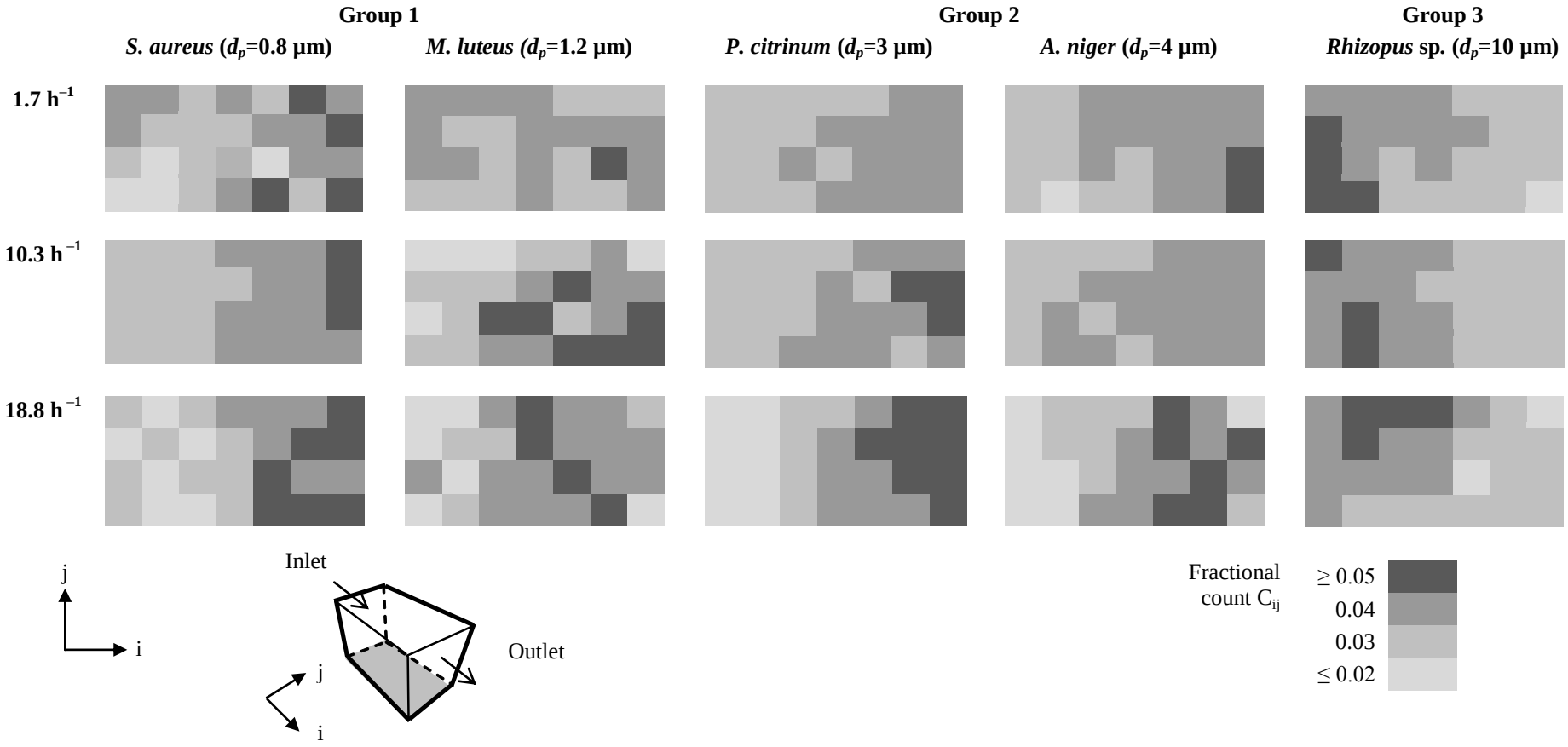

Figure 3. Average fractional counts (C_{ij}) measured on the agar plate array

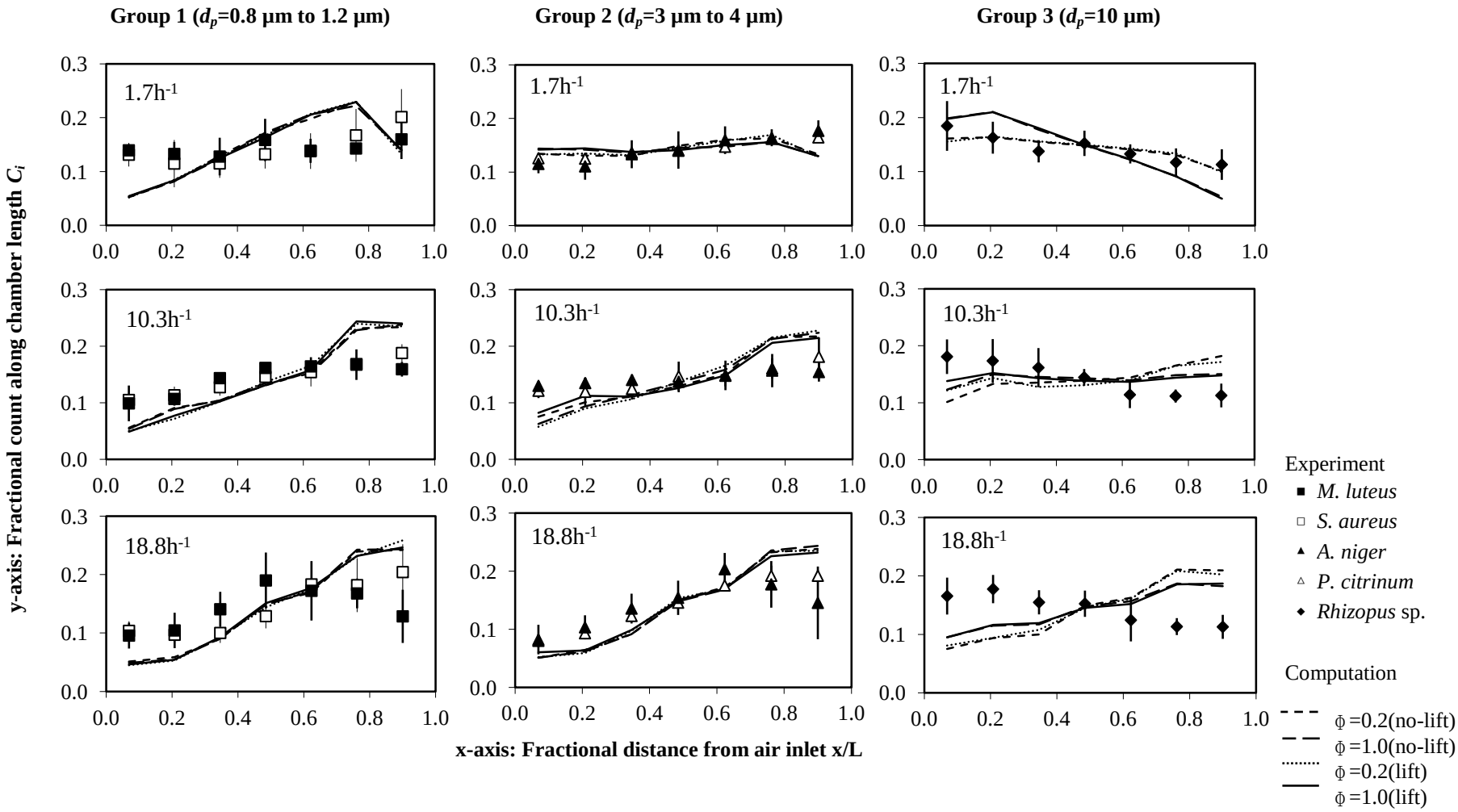

Figure 4. Longitudinal fractional counts C_i on the test chamber floor measured at three ventilations rates

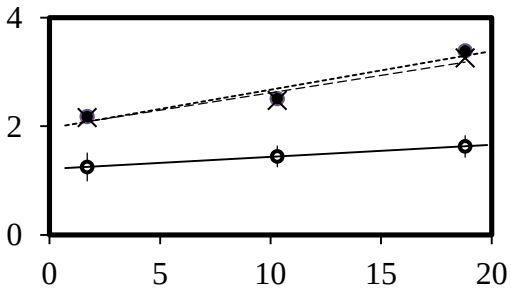

(a) Group 1 d_p=1 μm

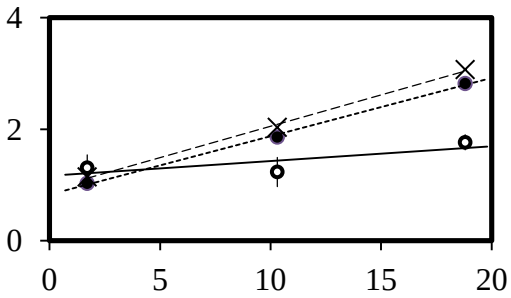

(b) Group 2 d_p=4 μm

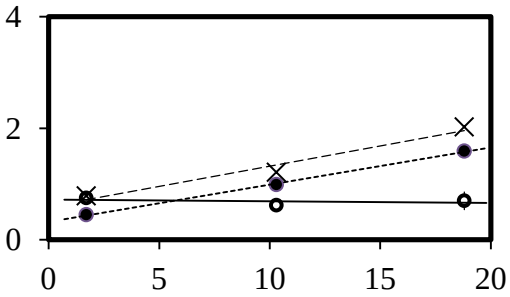

(c) Group 3 d_p=10 μm

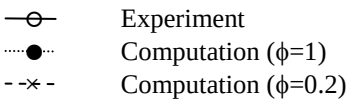

x-axis: ventilation rate V_R; y-axis: deposition ratio ω

Figure 5. Deposition ratios for the three tested microbial groups